Applied Catalysis B: Environmental 160–161 (2014) 106–114

Contents lists available at ScienceDirect

Applied Catalysis B: Environmental

journal homepage: www.elsevier.com/locate/apcatb

Formation of genotoxic quinones during bisphenol A degradation by TiO_2 photocatalysis and UV photolysis: A comparative study

A.O. Kondrakov[a,b,c,*], A.N. Ignatev[a,b], F.H. Frimmel[a], S. Bräse[c], H. Horn[a], A.I. Revelsky[b]

[a] Chair of Water Chemistry and Water Technology, Karlsruhe Institute of Technology, Engler-Bunte-Ring 1, Karlsruhe 76131, Germany
[b] Department of Chemistry, Moscow State University, Leninskie Gory 1-3, Moscow 119991, Russia
[c] Institute of Organic Chemistry, Karlsruhe Institute of Technology, Fritz-Haber-Weg 6, Karlsruhe 76131, Germany

ARTICLE INFO

Article history:
Received 8 March 2014
Received in revised form 29 April 2014
Accepted 3 May 2014
Available online 14 May 2014

Keywords:
Bisphenol A
TiO_2
Photocatalysis mechanism
Toxicity
Quinone

ABSTRACT

In this study, a hazardous DNA-binding agent, bisphenol A 3,4-quinone (BPAQ), was detected among products of bisphenol A (BPA) photocatalytic degradation. To clarify the mechanism of BPAQ formation, we investigated BPA degradation by TiO_2 photocatalysis and UV photolysis at 254 nm in detail. The main focus was given to understanding the roles of OH radicals and photogenerated holes in the evolution of potentially harmful aromatic products. Five new intermediates were identified using an enhanced LC–MS–MS/ToF approach. We found that direct hole oxidation was abundantly responsible for the transformations of BPA into quinone and catechol products. Scavenging of free OH radicals induced a mechanism change and intensified BPAQ formation. Direct UV photolysis produced two catechol derivatives with potentially lower endocrine-disrupting activity in comparison to BPA. Both of the processes demonstrated similar efficiencies in BPA elimination. Complete mineralization was achieved only in the case of TiO_2 photocatalysis, but accompanied by potentially genotoxic intermediates formed by hole oxidation.

1. Introduction

Bisphenol A (4,4′-(propane-2,2-diyl)diphenol, BPA) is one of the mostly produced organic chemicals and has various applications in polymer industry. Its global demand increased from 3.2 million tons in 2003 [1] to 5.2 million tons in 2008 [2]. BPA is an emergent environmental pollutant [3] and can cause diverse cellular responses even at low doses [4]. Particularly, it acts as an endocrine disruptor [5]. BPA has become ubiquitous in the environment. It was detected in landfill leachates, air, dust and waters [4]. Recently, the predicted no-effect concentration (PNEC) of BPA for the aquatic wildlife was revised and lowered from 100 $\mu g\,L^{-1}$ to 0.06 $\mu g\,L^{-1}$ [6]. Conventional biological wastewater treatment is inefficient for the elimination of low doses of BPA [7]. Consequently, continuous industrial and public discharges cause environmental BPA concentrations higher than PNEC values [7]. Photochemical processes, such as UV photolysis at 254 nm and TiO_2 photocatalysis demonstrated high efficiency in the treatment of BPA contaminated water [8–13]. Both of the processes usually transform dissolved pollutants to less harmful compounds [10,14]. However, in the case of BPA, the mixture of intermediate products formed before the complete mineralization may result in a higher estrogenic activity than BPA itself [15]. Recently, Kitamura et al. [16] pointed out, that *in vitro* and *in vivo* endocrine-disrupting activity of bisphenols is directly related to the molecular structure, particularly to the number and positions of hydroxyl groups in aromatic rings. So far, three main intermediates of BPA photocatalytic degradation by TiO_2 were reported [9,17–28]. 4-Hydroxyacetophenone was identified by LC–MS measurements using an authentic standard [29]. Two more molecular formulae were suggested [17]. Several identification techniques based on LC–MS data on molecular ion or GC–MS spectral data [9,18–20,29,30] were implemented, but no reliable structural information has been obtained. Moreover, no attempts to identify BPA products formed during direct UV photolysis at 254 nm were made. So, the overall estrogenic activities of the BPA solutions treated by UV photolysis and/or TiO_2 photocatalysis were measured [14,15], but knowledge on the degradation mechanisms remains deficient. Therefore, obtaining of structural information on aromatic and particularly phenolic products of BPA photodegradation is an issue of high importance.

This is a comparative study of BPA degradation by TiO_2 photocatalysis and UV photolysis at 254 nm, with the main focus on

* Corresponding author at: Karlsruhe Institute of Technology, Chair of Water Chemistry and Water Technology, Engler-Bunte-Ring 1, 76131 Karlsruhe, Baden-Württemberg, Germany. Tel.: +49 721 608 47057; fax: +49 721 608 47051.
E-mail address: aleksandr.kondrakov@kit.edu (A.O. Kondrakov).

http://dx.doi.org/10.1016/j.apcatb.2014.05.007
0926-3373/

the mechanisms of aromatic products formation. Identification of the intermediates was performed by means of LC–MS–MS and LC–MS–ToF methods. Once intermediates were identified, their endocrine-disrupting activity and toxicity were evaluated on the base of literature data. Kinetics of both the processes were compared, and the role of OH radical was investigated in experiments with and without tertiary butanol (tBuOH). The contribution of hole oxidation to the overall degradation of BPA and formation of aromatic products was assessed as well. In addition, we estimated quantum yields of BPA removal and mineralization and correlated the results with the oxidants concentrations.

2. Experimental

2.1. Materials and apparatus

TiO_2 (Aeroxide P25, former name Degussa P25) was purchased from Evonik, Hanau, Germany. Ultrapure water was generated by a Purelab flex device (ELGA, Celle, Germany) out of distilled water and was used in all experiments. BPA (purity 99%) was obtained from Sigma-Aldrich, Steinheim, Germany. tBuOH from VWR, Bruchsal, Germany (purity min. 99.5%), was additionally distilled before the experiments. Stock solution of uridine (purity min. 99%, Sigma-Aldrich, Steinheim, Germany), used for the actinometry, was prepared directly before the measurements. Working solutions of uridine were prepared using phosphate buffer (KH_2PO_4 and Na_2HPO_4 from Merck, Darmstadt, Germany). All the organic solvents were HPLC grade.

The degradation experiments were conducted in a 200 mL reactor equipped with a coaxial quartz tube, a pH-electrode, an aeration inlet and an outlet for CO_2 sampling (Fig. 1). The reactor was filled to 180 mL. The solution/suspension was constantly mixed with a magnetic stirrer. The dissolved oxygen concentration was kept constant by continuous aeration with CO_2-free synthetic air. For this, the aeration inlet, equipped with an aluminum diffuser, was connected to a gas tank through a flow controller. The gas flow was adjusted to 0.21 L min^{-1} and remained constant in all the experiments. The reactor temperature was controlled by passing water thermostated to 20 °C through an outer jacket of the reactor. The quartz tube and a UV lamp were cooled by the air flow of room temperature. The low-pressure ozone-free UV Hg lamp (UVI 40 4C, UV-Technik Meyer, Ortenberg, Germany), equipped with the doped quartz to cut off the VUV irradiation (λ = 184.9 nm), had monochromatic spectrum at λ = 254 nm and 4 μE s^{-1} irradiance measured by uridine actinometry [31]. The lamp was turned on for 30 min before every experiment to reach the thermal equilibrium. Stability of UV intensity was checked with a digital UV radiometer (Epigap Optronic GmbH, Germany) according to [32]. The actinometry was repeated five times to estimate the irradiance deviation, which was 10%.

The TiO_2 load was 0.1 mg L^{-1} in all the experiments, as the optimal concentration in terms of the efficiency of light absorption and catalyst demand [28,33,34]. Organic impurities on TiO_2 surface were removed by 12 h. calcination at 300 °C. After 30 min sonication of the photocatalyst suspension the aliquot of BPA stock solution was added. The mixture was kept in dark for 30 min to reach adsorption equilibrium [35]. The initial BPA concentration of 220 μM was chosen to maximize the coverage of the photocatalyst surface by BPA molecules [36]. Typically, BPA in aqueous media exists in the unionized form ($pK_{a\,I}$ = 9.6, $pK_{a\,II}$ = 10.2 [37]). pH has a slight effect on BPA adsorption on TiO_2 [38]. Therefore, the media was not buffered, but pH was monitored throughout the experiments. pH varied between 4.7 and 6.7 with the initial value of 6.7. Conditions for all the photolytic and photocatalytic experiments were identical.

A peristaltic pump continuously pumped the suspension through a capillary tube cycle. To take a sample for LC–MS measurements the cycling was interrupted with a valve, and 1 mL of the suspension was collected in a plastic Eppendorf tube. The sampling took around 20 s. In the case of photocatalytic experiments, the samples were centrifuged before the analysis to separate the TiO_2 suspension. The effect of tBuOH (54 mM) on the rates of UV photolysis and photocatalysis was estimated by conducting three replicates.

2.2. Analytical methods

An HPLC chromatograph Agilent 1100 with a Diode Array Detector (Agilent Technologies, Waldbronn, Germany) was used for HPLC-UV measurements to quantify BPA. UV absorbance was measured between 200 and 400 nm with 2 nm step and 2 nm s^{-1} scan rate. HPLC chromatograms at 280 nm were used for calibration and quantitative analysis. LC–MS–ToF measurements were done using an Agilent 1290 HPLC system coupled with a 6540 UHD Q-ToF mass spectrometer (Agilent Technologies, Waldbronn, Germany) operated in negative ionization mode. LC–MS–MS measurements were performed using the chromatograph Agilent 1100 coupled with a triple quadrupole mass-spectrometric detector Applied Biosystems 3000 (MDS Sciex Instruments, Concord, ON, Canada). MS–MS fragmentation was carried out at −30 eV and −60 eV in negative ionization mode. All the HPLC measurements were conducted using a 125-4 mm LiChrospher C-18 5 μm column (Merck Milipore, Schwalbach, Germany). Sample injection volume was 100 μL. The column was eluted with 5–95% linear gradient of acetonitrile in water buffered by ammonium acetate (2%) at a rate of 0.5 mL min^{-1}.

Experimental logP coefficients of intermediates were calculated out of their HPLC retention times (RT) by the use of a "logP–RT" correlation. The correlation was preliminary established using RT of standards with known logP values (see Supplementary data). The inaccuracy was estimated on the basis of RT deviations in replicates. The estimations of logP values for structure candidates were done according to the principle of isolating carbons [39] using ACD/Chemsketch software. The structures of the proposed intermediates were then chosen among possible isomers according to the best matches between predicted and experimentally measured logP coefficients. LC–MS data analysis was performed in ACD/Spectrus Processor software.

Concentration of CO_2, formed during the degradation, was measured in the gas, exciting the reactor, by an infrared CO_2 detector Ultramat 5 (Siemens, Germany). For this, CO_2-free synthetic air was used for the aeration. The complete CO_2 degassing of the solution was checked prior to every experiment. The gas samples were taken using a gastight syringe. Details of the analysis can be found in Supplementary data. To ensure stability of the suspension during photocatalytic reaction, zeta potential of the TiO_2 particles was monitored with using laser Doppler microelectrophoresis measured by Zetasizer Nano ZS (Malvern) analyzer (see Supplementary data).

3. Results and discussion

3.1. BPA removal and mineralization

To understand formation kinetics of BPA intermediates, evolution of organic carbon was investigated. For this, BPA and CO_2 concentrations were monitored throughout the reactions. The concentration of organic carbon contained in intermediates was then calculated out of the carbon balance as follows:

$$C_{org.carb.} = 15 \times C_{BPA} - C_{CO_2,aq.} \quad (1)$$

where $C_{org.carb.}$ is the total concentration of organic intermediates in terms of moles of carbon (M); C_{BPA} is concentration of BPA; $C_{CO_2,aq.}$ is total amount of CO_2, generated at a time of interest, divided

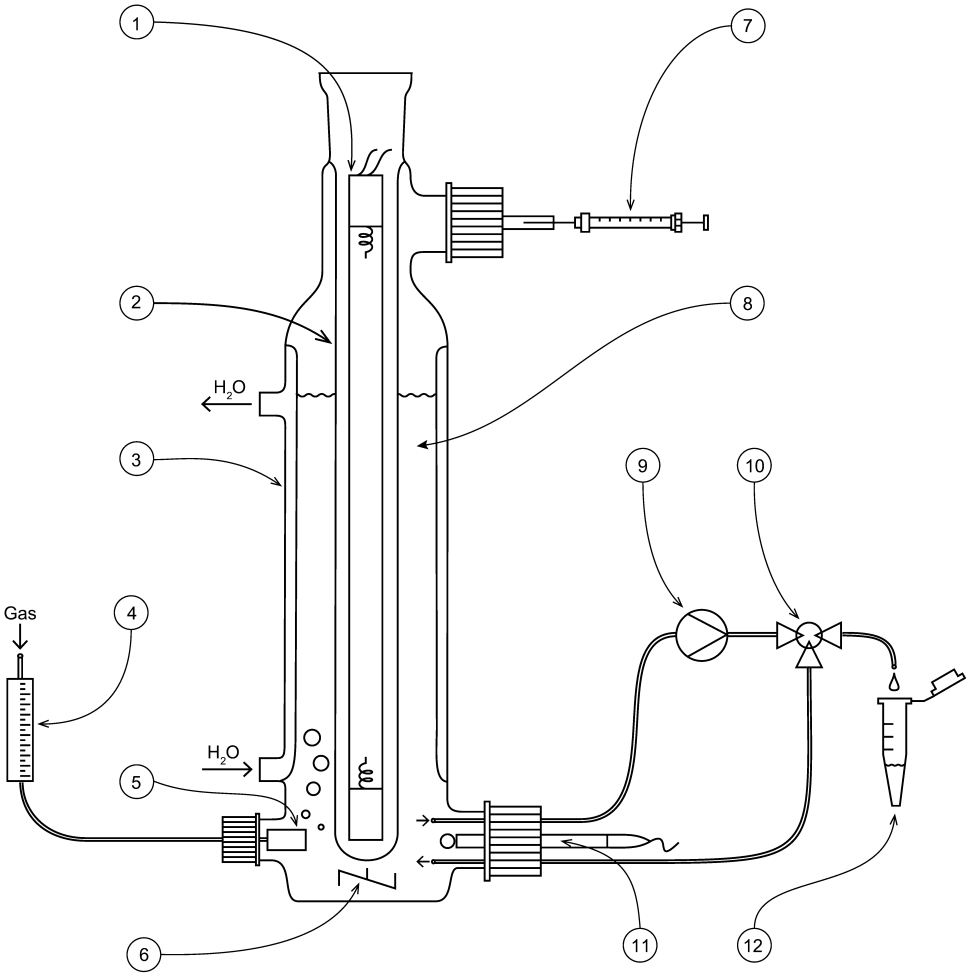

Fig. 1. UV photolysis/photocatalysis reactor used for BPA degradation. (1) UV lamp; (2) quartz tube; (3) thermostating jacket; (4) gas flow meter; (5) gas diffuser; (6) magnetic stirrer; (7) gastight syringe for CO_2 sampling; (8) BPA solution; (9) sampling pump with capillary tubes; (10) sampling valve; (11) pH electrode; (12) plastic Eppendorf tube for solution/suspension samples.

by the solution volume (See Supplementary data for details of the calculation).

The carbon balance for UV photolytic and TiO_2 photocatalytic degradation of BPA is shown in Fig. 2. The UV photolysis achieved complete removal of BPA after 130 min of the treatment. It agreed with the previous findings [14]. However, only 12% of the organic carbon were transformed into CO_2 at 240 min of the treatment. HPLC-UV measurements demonstrated, that the photolysis products absorbed no UV light at 254 nm; therefore, complete mineralization was not expected.

BPA was completely decomposed by TiO_2 photocatalysis in 45 min, and full mineralization was achieved in 240 min. Apparently, the mineralization was reached due to generation of sufficient amounts of OH radical and photogenerated holes, as these

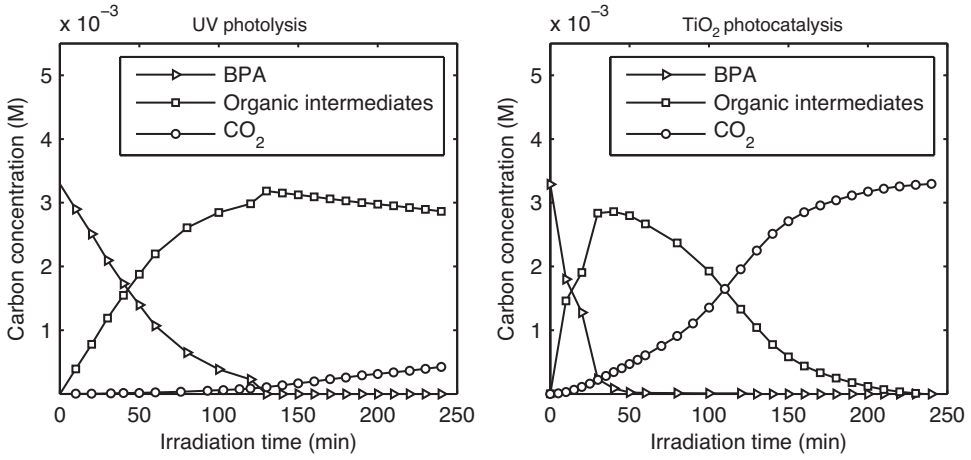

Fig. 2. Carbon balance for BPA degradation by UV photolysis and TiO_2 photocatalysis (C_0 (BPA) = 0.2 mM, I_0 = 4 μE s^{-1}, ρ (TiO_2) = 0.1 g L^{-1}, pH 7, T = 25 °C).

Table 1
Quantum yields of BPA removal and mineralization.

	$\Phi_{removal}$	$\Phi_{mineralization}$
UV photolysis	0.0039 ± 0.0004	–
TiO_2 photocatalysis	0.0044 ± 0.0005	$(8.7 \pm 0.7) \times 10^{-4}$

species are highly reactive towards most of organic compounds [40].

Since UV photolysis did decompose and partially mineralize BPA, it was necessary to evaluate its contribution to photocatalytic treatment with TiO_2. In the presence of TiO_2, BPA absorbs much less amounts of UV light, than in the absence of TiO_2, thus the rate of its photolytic decay can be significantly decreased. To evaluate the fraction of UV irradiation absorbed by BPA in the presence of TiO_2, the inner filter model [41] was used:

$$F_{BPA} = \frac{\mu_{BPA}\rho_{BPA}}{\mu_{BPA}\rho_{BPA} + \mu_{TiO_2}\rho_{TiO_2}} \quad (2)$$

where F_{BPA} is the fraction of light absorbed by BPA; μ_{BPA} and μ_{TiO_2} are mass extinction coefficients of BPA and TiO_2 ($g\,L^{-1}\,cm^{-1}$), respectively; ρ_{BPA} and ρ_{TiO_2} are mass concentrations of BPA and TiO_2 ($g\,L^{-1}$), correspondingly. We assumed that only BPA and TiO_2 absorbed UV light and neglected the absorption by other compounds.

For 254 nm UV light $\mu_{BPA} = 1.9$ g L^{-1} cm^{-1} and $\mu_{TiO_2} = 12.5$ g L^{-1} cm^{-1} [35,36]. In our photocatalysis experiments $\rho_{BPA} = 0.05$ g L^{-1} and $\rho_{TiO_2} = 0.1$ g L^{-1}. Under these conditions, according to Eq. (2), BPA absorbed only 7% of UV light, and 93% were absorbed by TiO_2. Consequently, BPA degradation was mainly driven by photogenerated holes and OH radicals.

To compare efficiencies of photolytic and photocatalytic removal of BPA, the corresponding quantum yields were calculated. The quantum yield (Φ) of a photochemical process is defined as the ratio of the moles of transformed molecules to the moles of photons absorbed, or alternatively:

$$\Phi = \frac{\Delta n}{\Delta t} \times I_{abs}^{-1} \quad (3)$$

where $\Delta n/\Delta t$ is the rate of a photochemical transformation ($mol\,s^{-1}$); I_{abs} is the intensity of absorbed light ($E\,s^{-1}$).

The calculated quantum yields showed that both the processes have nearly equal efficiencies in BPA removal (Table 1).

Since photodecomposition of an organic molecule requires absorption of a photon by the molecule, the performance of a photolytic treatment strongly depends on the properties of the compound. In this way, accumulation of organic carbon during photolysis can be explained by formation of products which did not absorb UV light at 254 nm as strongly as BPA. Therefore, significant amounts of organic intermediates still remained in the solutions even when BPA conversion reached high levels.

3.2. LC–MS identification of intermediates

The samples for the LC–MS–ToF screening were taken at 120 min of the UV photolytic and at 30 min of the photocatalytic treatment, respectively. As can be seen in Fig. 2, these time points corresponded to the highest concentration of organic intermediates.

The screening displayed pseudomolecular ions at *m/z* 243 and 167 for UV photolysis intermediates and at *m/z* 243, 259, 241, 257, 245, 261 and 167 for intermediates of TiO_2 photocatalysis. The exact molecular masses of these ions, delivered by LC–MS–ToF technique, allowed us to obtain unambiguous elemental compositions for all the detected substances. The structures of the intermediates were chosen among possible isomers according to best matches between the estimated and experimentally measured log*P* coefficients (for details, see Section 2.2). Main LC–MS data are presented in Table 2. For short here and further the intermediates are numbered from **1** to **7**. For detailed LC–MS data and information on interpretation of LC–MS–MS spectra, please refer to Supplementary data.

Structures of the intermediates identified are depicted in Fig. 3. Compound **1** with $[M—H]^-$ at *m/z* 243 was identified as BPA catechol, which is known as a primary product of BPA degradation by TiO_2 photocatalysis [17,20–23]. Ion at *m/z* 259 was identified as $[M—H]^-$ of BPA dicatechol (structure **2**). Previously it had been detected in BPA solution treated by TiO_2 photocatalysis coupled with high-frequency ultrasound [23]. The elemental composition of the $[M—H]^-$ ions at *m/z* 241 and 257 suggested them to be quinone derivatives of BPA and BPA dicatechol (structures **3** and **4**, respectively). $[M—H]^-$ ions at *m/z* at 261, 245 and 167 were attributed to 4,4′-(1-hydroxyethane-1,1-diyl) dicatechol, 4,4′-ethane-1,1-diyldicatechol and 4-(2-hydroxypropan-2-yl) catechol (structures **5–7**, respectively).

Structures **3–7** have not been reported before. Remarkably, structures **1** and **7** were detected in both the photolytic and the photocatalytic processes. This observation will be discussed in Section 3.5.

3.3. Hazard assessment of the intermediates

In this study, two products of BPA photolysis and seven products of BPA photocatalysis were identified (Fig. 3). Structures **3–7** had not been reported as intermediates of BPA degradation. In this connection, literature was examined with a focus on endocrine-disrupting activity and toxicity of the intermediates identified for the first time.

3,4-Quinone of BPA (structure **3**), formed only in TiO_2 photocatalysis, acts as DNA binding agent [42–44]. Metabolic activation of BPA can provoke formation of DNA adducts in rat prostate cells, rat liver and mice mammary tissue [44–46]. Particularly, formation of such adducts were related to the covalent modifications in DNA

Table 2
LC–MS and logP data of the intermediates detected in BPA solutions treated by UV photolysis and TiO_2 photocatalysis.

Structure no.	$[M—H]^-$	Formula	Mass fragments	$logP_{exp}$	$logP_{calc}$	Process		Previously reported
						UV	UV + TiO_2	
1	243.1026	$C_{15}H_{16}O_3$	228-149-167-124	2.9 ± 0.1	2.83 ± 0.24	+	+	Yes [12,15–18]
2	259.0975	$C_{15}H_{16}O_4$	244-228-109	2.5 ± 0.1	2.23 ± 0.25	–	+	Yes [18]
3	241.0870	$C_{15}H_{14}O_3$	226-211-198-185-171-133-121-107-93	3.2 ± 0.1	2.54 ± 0.39	–	+	No
4	257.0819	$C_{15}H_{14}O_4$	242-227-214-201-189	2.7 ± 0.1	0.98 ± 0.6	–	+	No
5	245.0819	$C_{14}H_{14}O_4$	227-209-109	1.4 ± 0.1	1.88 ± 0.24	–	+	No
6	261.0768	$C_{14}H_{14}O_5$	243-149	0.9 ± 0.1	1.29 ± 0.33	–	+	No
7	167.0713	$C_9H_{12}O_3$	149-134-124-121	0.6 ± 0.1	0.39 ± 0.24	+	+	No

induced by BPA 3,4-quinone [44]. No information on hydroxylated derivative of 3,4-quinone of BPA (structure **4**) was found.

Direct 254 nm UV photolysis was reported to be able to decrease the overall estrogenic activity of BPA solution [14]. We detected only two products of BPA photolytic degradation, which may be estrogenic active due to their phenolic structures [16]. They were BPA catechol (structure **1**) and 4-(2-hydroxypropan-2-yl)-catechol (compound **7**). BPA catechol has a weak estrogenic activity, which is approximately three times lower, than that of BPA in MCF-7 cells [47]. Thus, we concluded that the estrogenic activity of compound **7** may be lower, comparing to BPA, as well.

We assumed that all the intermediates, which have hindered hydroxyl groups in aromatic ring (structures **2** and **6**) or hydroxylated propane group (structures **5** and **7**), are less estrogenic active than BPA. This assumption was based on the data on estrogenic activity of BPA-related compounds in ovariectomized mice and MCF-7 cells obtained by Kitamura et al. [16]. They figured out, that phenolic hydroxyl group and propane bridge group are essential for interactions with a binding pocket of estrogen receptor. Particularly, introduction of an additional hydroxyl groups into the aromatic ring or hydroxylation of the propane bridge group decreased the estrogenic activity [16].

To sum up, we believe that the catechol derivatives of BPA (structures **1** and **7**), formed during direct UV photolysis, should not increase the estrogenic activity of initial solution [14,16]. But the quinone derivatives of BPA (structures **3** and **4**) should receive more attention, since such compounds are potential mutagens [42–44].

Table 3
Effect of tBuOH on the rates of BPA removal by UV photolysis and TiO_2 photocatalysis.

Process	C_{tBuOH} (M)	Rate constant (min^{-1})	R^2
UV photolysis	0	0.0186	0.9860
	0.054	0.0144	0.9979
TiO_2 photocatalysis	0	0.0973	0.9698
	0.054	0.0254	0.9988

3.4. The role of OH radical in BPA elimination

To reveal the role of OH radical in the elimination of BPA, photolytic and photocatalytic experiments were carried out in the presence of *t*BuOH as a radical scavenger [48]. *t*BuOH does not absorb 254 nm UV light, but can efficiently deactivate free OH radicals in bulk solution and inhibit radical oxidation of dissolved compounds.

Our results showed that *t*BuOH retarded photolytic and photocatalytic decays of BPA, which indicated formation of free OH radicals in both the processes. The reaction kinetics were fitted with first order kinetics. The corresponding experimental rate constants of BPA disappearance are presented in Table 3. We assumed that free OH radicals were completely scavenged in the presence of

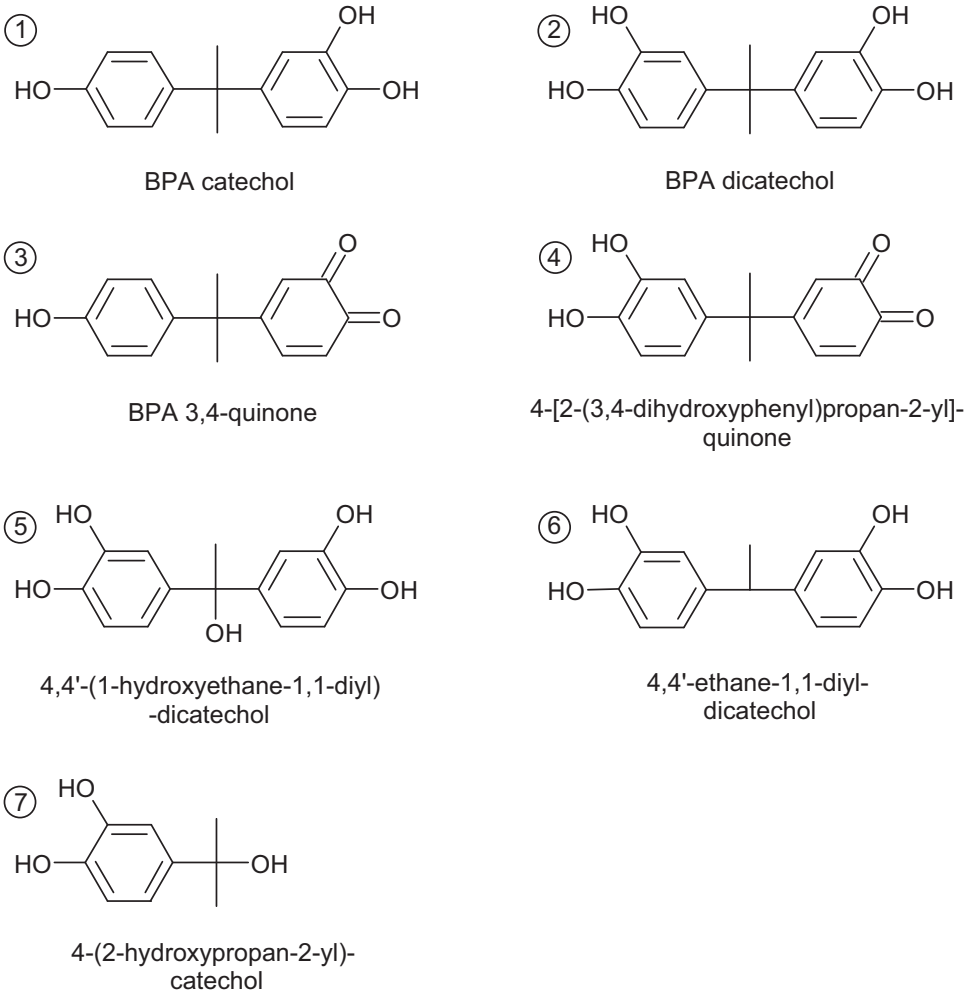

Fig. 3. Intermediates formed during TiO_2 photocatalysis (**1**–**7**) and UV photolysis (**1**, **7**).

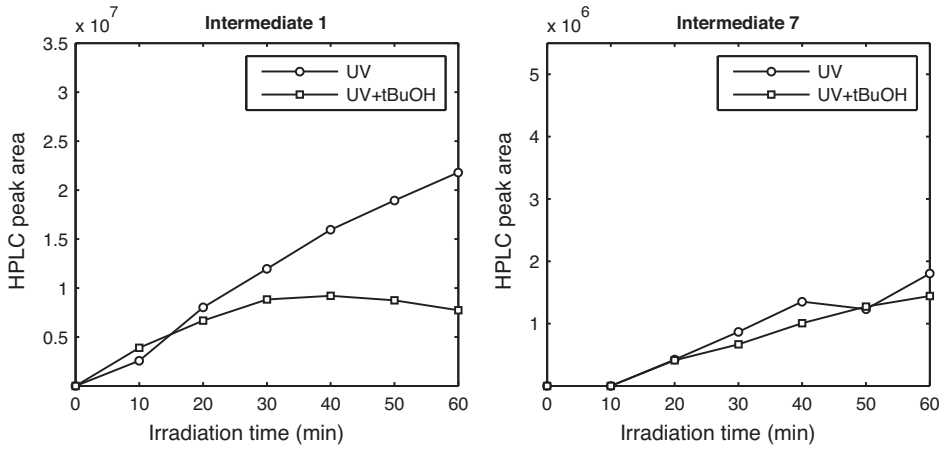

Fig. 4. Kinetic profiles of major intermediates formed during direct UV photolysis of BPA. (C_0 (BPA) = 0.2 mM, I_0 = 4 μE s^{-1}, pH 7, T = 25 °C).

0.054 M *t*BuOH and used the inhibition effect for their quantification. For the UV photolysis OH radical concentration was calculated as follows:

$$C_{OH} = \frac{k^{I}_{BPA} - k^{I}_{BPA/tBuOH}}{k^{II}_{BPA-OH}} \quad (4)$$

where C_{OH} is the concentration of the free OH radicals (M); k^{I}_{BPA} and $k^{I}_{BPA/tBuOH}$ are the apparent first order rate constants of BPA disappearance in absence and presence of *t*BuOH, respectively (min^{-1}); k^{II}_{BPA-OH} is the second order rate constant for the reaction of BPA with OH radical (M^{-1} min^{-1}).

Concentration of free OH radicals, generated during UV photolysis, according to Eq. (4), was $C_{OH} = 7 \times 10^{-15}$ M. There are two types of OH radicals in the TiO_2 photocatalytic process: surface bound OH radicals, generated out of adsorbed H_2O by photogenerated valence band holes, and free OH radicals in bulk solution. Indeed, surface bound OH radicals are undistinguishable from the valence band holes [49], so we used the term "hole" for both. tBuOH adsorption on TiO_2 is rather low [15], therefore it scavenges mainly free OH radicals. More rigorously, competition of tBuOH and BPA for valence

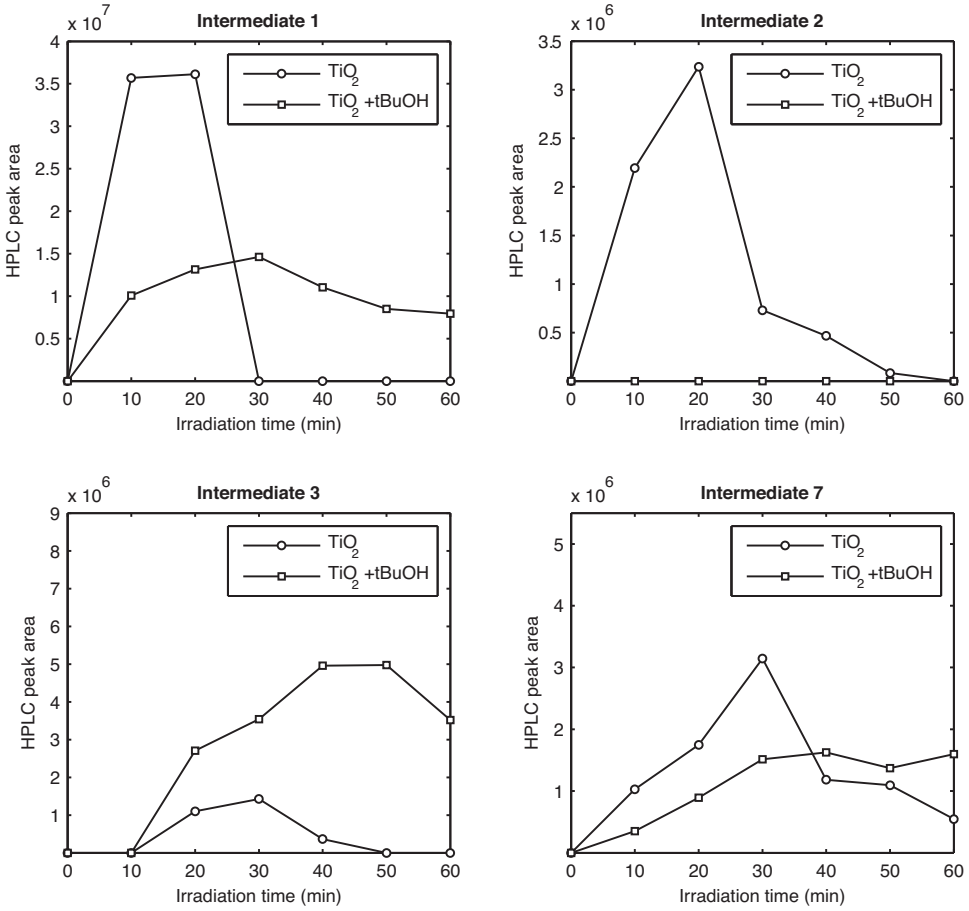

Fig. 5. Kinetic profiles of major intermediates formed during photocatalytic degradation. (C_0 (BPA) = 0.2 mM, I_0 = 4 μE s^{-1}, ρ (TiO_2) = 0.1 g L^{-1}, pH 7, T = 25 °C).

band holes can be evaluated by means of Langmuir–Hinshelwood model [48]:

$$F_{surf} = \frac{k^{II}_{tBuOH-h^+} K_{tBuOH} C_{tBuOH}}{k^{II}_{tBuOH-h^+} K_{tBuOH} C_{tBuOH} + k^{II}_{BPA-h^+} K_{BPA} C_{BPA}} \quad (5)$$

where F_{surf} is the fraction of holes, reacted with tBuOH; $k^{II}_{tBuOH-h^+}$ and $k^{II}_{BPA-h^+}$ are the second order rate constants for the reactions of holes with *t*BuOH and BPA ($M^{-1}\ s^{-1}$); K_{tBuOH} and K_{BPA} are Langmuir constants of *t*BuOH and BPA adsorption on TiO_2 surface (M^{-1}); C_{tBuOH} and C_{BPA} are concentrations of *t*BuOH and BPA in bulk solution (M).

We assumed that the reactions of BPA and *t*BuOH with the holes proceeded with the same rate constants as for the reactions of BPA and *t*BuOH with free OH radicals. Substitution of the values $k^{II}_{tBuOH-h^+} = 5.0 \times 10^8\ M^{-1}\ s^{-1}$ [45], $k^{II}_{BPA-h^+} = 6.0 \times 10^9\ M^{-1}\ s^{-1}$ [46], $K_{tBuOH} = 17\ M^{-1}$ [14], $K_{BPA} = 3.7 \times 10^5\ M^{-1}$ [24], $C_{tBuOH} = 0.054$ M and $C_{BPA} = 2 \times 10^{-4}$ M in Eq. (5) gave $F_{surf} = 10^{-3}$. So, only 0.1% of the holes were scavenged by tBuOH in the photocatalysis experiment. Thus, we applied Eq. (4) to quantify free OH radicals formed in the TiO_2 suspension and obtained $C_{OH} = 1.2 \times 10^{-13}$ M. Further, concentration of holes (C_{h^+}), generated on the TiO_2 surface was calculated as follows:

$$C_{h^+} = \frac{k^{I}_{BPA/tBuOH}}{k^{II}_{BPA-OH}} \quad (6)$$

Eq. (6) gave $C_{h^+} = 1.36 \times 10^{-14}$ M. This value corresponded to 10% of the total oxidants concentration and agreed with moderate BPA adsorption capacity of P25 reported before [38]. Concentration

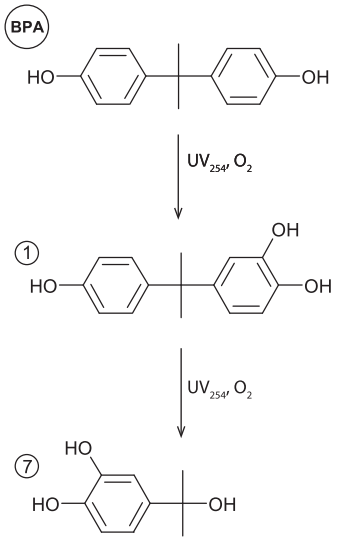

Fig. 6. Mechanism of BPA degradation by UV photolysis.

of reactive oxidants, *e.g.* OH radicals and holes, generated in the photocatalytic process, were almost two orders of magnitude higher than in the case of photolysis. These results explained the enhanced efficiency of photocatalytic mineralization. Nevertheless, the amounts of OH radicals generated during UV photolysis contributed to the BPA degradation rate by 23% (Table 3) and apparently provided partial mineralization (Fig. 2).

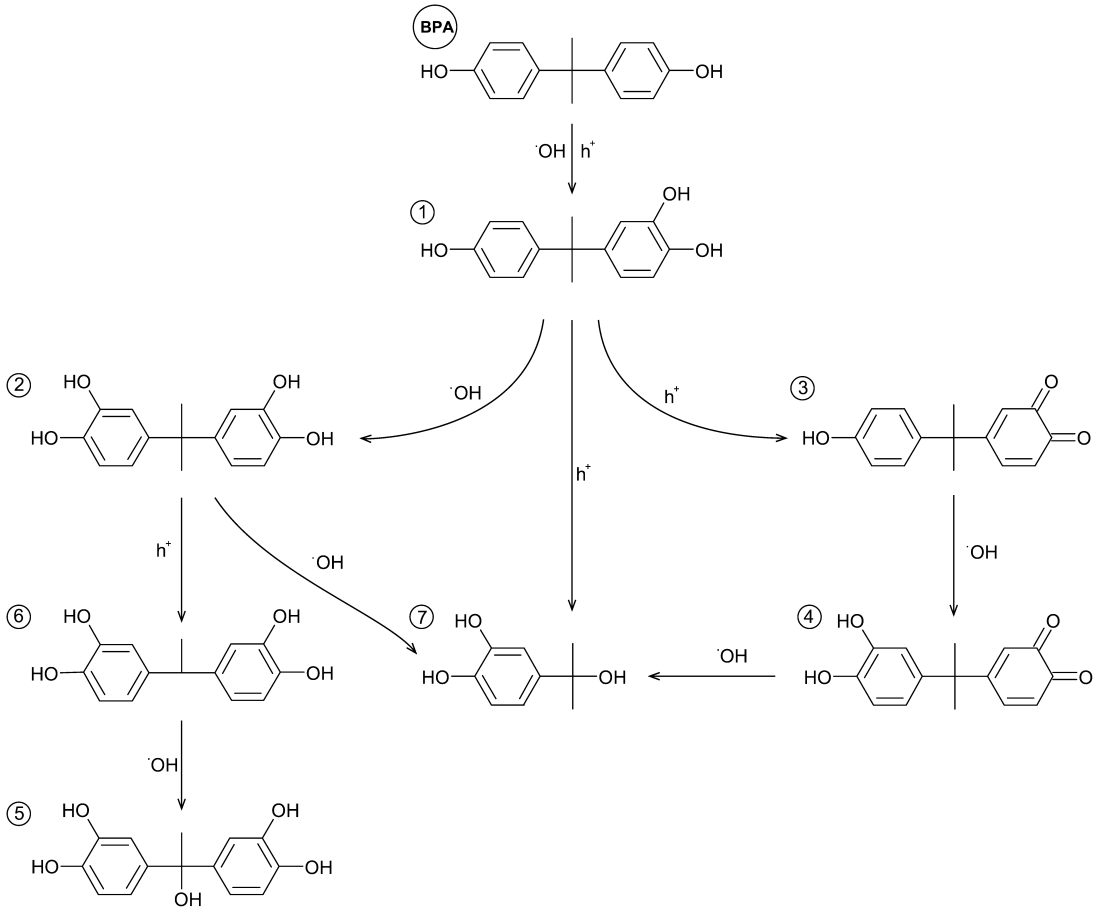

Fig. 7. Mechanism of BPA degradation by TiO_2 photocatalysis.

3.5. Degradation mechanisms

To understand the pathways of BPA elimination, we monitored the formation kinetics of major intermediates **1**–**3** and **7** during both of the processes. Special attention was paid to potentially genotoxic 3,4-quinone of BPA (structure **3**), generated during photocatalytic treatment. Since no standards of the products identified were available, profiles "HPLC-UV peak area vs. time of irradiation" were analyzed. The HPLC profiles in Figs. 4 and 5 cover the first 60 min of the degradation. In the experiments with the scavenger high initial concentration of tBuOH provided complete deactivation of free OH radicals during this time.

Formation of intermediates **1** and **7** during UV photolysis was slightly affected by tBuOH (Fig. 4). It indicated that their generation was driven by direct photolytic cleavage of a BPA molecule with subsequent oxidation by dissolved oxygen.

In the case of TiO_2 photocatalysis, the influence of direct UV photolysis was negligible (see Section 3.1), and the main oxidizing agents were OH radicals and photogenerated holes. Kinetic profiles shown in Fig. 5 illustrate that catechol and quinone intermediates were formed, even when all free OH radicals were suppressed. This is a clear evidence that hole oxidation was one of the main pathways of catechol and quinone production. Moreover, scavenging of free OH radicals led to blockage of BPA dicatechol formation, but favored generation of BPA 3,4-quinone. Evidently, BPA catechol was a precursor of BPA quinones [47], so we observed competition between holes and OH radicals for the catechol oxidation. We concluded that photogenerated holes were responsible for the transformation of BPA catechol into BPA quinone, while free OH radicals hydroxylated BPA catechol to BPA dicatechol.

Finally, the mechanisms of BPA degradation by UV photolysis (Fig. 6) and TiO_2 photocatalysis (Fig. 7) were compiled. UV photolysis resulted in rapid formation of BPA catechol (structure **1**) and 4-(2-hydroxypropan-2-yl)-catechol (structure **7**) that have lower estrogenic-disrupting activity comparing to BPA [14,16]. Free OH radicals, probed by tBuOH, provided partial mineralization of organic carbon. But their concentration (see Section 3.4) was not enough to provide full mineralization during the photolysis.

It should be noted that TiO_2 photocatalysis also led to generation of intermediates **1** and **7**. We explained this observation in terms of similar mechanisms of oxidation of phenolic compounds by OH radical and UV light. OH radical readily attacks an electron-rich aromatic ring of a BPA molecule, forming a cyclohexadienyl radical [50]. If absorption of a photon takes place, it results in formation of phenoxy radical of BPA [51]. In presence of oxygen, both cyclohexadienyl and phenoxy BPA radicals can be further hydroxylated to intermediates **1** and **7**.

Oxidation of BPA by TiO_2 photocatalysis was driven by holes and OH radicals and resulted in formation of seven intermediates. Scavenging of free OH radicals caused a mechanism change and intensified formation of potentially genotoxic 3,4-quinone of BPA. Intermediate **7** was the most stable aromatic compound formed in the photolytic and photocatalytic treatment. However, it was not detected after 120 min of TiO_2 photocatalytic treatment and 240 min of UV photolysis. During this time period, all the aromatic intermediates were degraded, and pH dropped. Products formed afterwards, were assumed to be nonaromatic acids.

4. Conclusions

LC–MS methods are widely used for obtaining structural information of products formed during photochemical oxidation processes. In this study, a combination of LC–MS–ToF, LC–MS–MS and logP estimations, based on the principle of isolated carbons, showed high performance in the investigation of intermediate products of BPA oxidation by UV photolysis at 254 nm and TiO_2 photocatalysis.

The enhanced analytical approach allowed us to identify five new potentially toxic intermediates (*e.g.* genotoxic 3,4-quinone of BPA) and to clarify the pathways of BPA degradation. This study demonstrated that oxidation of BPA on TiO_2 surface by holes and its hydroxylation by free OH radicals in the solution are two interconnected pathways, which cannot be considered independently. It emphasizes the complexity of the photocatalytic degradation of BPA and opposes it to UV photolysis, whose mechanism is relatively explicit. On the basis of these observations UV photolysis may look more feasible for practical applications.

Systematic monitoring of the toxicity and the content of quinone products at different operating conditions have to be done prior to the real application of the photocatalytic method. Particularly, further experimentations with hole scavengers will complement the gained knowledge on BPA transformations on photogenerated holes. These studies may help to avoid formation of undesirable products, like genotoxic BPA 3,4-quinone, and will assist further development of the photocatalytic treatment.

Acknowledgments

The authors gratefully acknowledge the financial support of the state Baden-Württemberg by ZO IV research program "Innovation und Exzellenz: Beherrschung komplexer Systeme". The research group also thanks Karlsruhe Technologiezentrum Wasser for conducted LC–MS–ToF measurements and Advanced Chemistry Development, Inc. for the support with software licensing.

Appendix A. Supplementary data

Supplementary material related to this article can be found, in the online version, at http://dx.doi.org/10.1016/j.apcatb.2014.05.007.

References

[1] W.-T. Tsai, J. Environ. Sci. Health, Part C Environ. Carcinog. Ecotoxicol. Rev. 24 (2006) 225–255.
[2] ICIS, Use and Market Data, ICIS, 2008, Available online at: http://www.icis.com/Articles/2008/01/14/9092025/chemical-profile-bisphenol-a.html.
[3] H. Fromme, T. Küchler, T. Otto, K. Pilz, J. Müller, A. Wenzel, Water Res. 36 (2002) 1429–1438.
[4] S. Flint, T. Markle, S. Thompson, E. Wallace, J. Environ. Manage. 104 (2012) 19–34.
[5] L.N. Vandenberg, T. Colborn, T.B. Hayes, J.J. Heindel, D.R. Jacobs, D.H. Lee, T. Shioda, A.M. Soto, F.S. vom Saal, W.V. Welshons, R.T. Zoeller, J.P. Myers, Endocr. Rev. 33 (2012) 378–455.
[6] M. Wright-Walters, C. Volz, E. Talbott, D. Davis, Sci. Total Environ. 409 (2011) 676–685.
[7] Y. Zhang, J.L. Zhou, Chemosphere 73 (2008) 848–853.
[8] C. Baeza, D.R.U. Knappe, Water Res. 45 (2011) 4531–4543.
[9] E.M. Rodríguez, G. Fernández, N. Klamerth, M.I. Maldonado, P.M. Álvarez, S. Malato, Appl. Catal., B: Environ. 95 (2010) 228–237.
[10] M.N. Chong, B. Jin, C.W.K. Chow, C. Saint, Water Res. 44 (2010) 2997–3027.
[11] S.-M. Lam, J.-C. Sin, A.Z. Abdullah, A.R. Mohamed, Ceram. Int. 39 (2013) 2343–2352.
[12] I. Gültekin, N.H. Ince, J. Environ. Manage. 85 (2007) 816–832.
[13] W.-T. Tsai, M.-K. Lee, T.-Y. Su, Y.-M. Chang, J. Hazard. Mater. 168 (2009) 269–275.
[14] M. Neamţu, F.H. Frimmel, Water Res. 40 (2006) 3745–3750.
[15] K. Chiang, T.M. Lim, L. Tsen, C.C. Lee, Appl. Catal., A: Gen. 261 (2004) 225–237.
[16] S. Kitamura, T. Suzuki, S. Sanoh, R. Kohta, N. Jinno, K. Sugihara, S.i. Yoshihara, N. Fujimoto, H. Watanabe, S. Ohta, Toxicol. Sci. 84 (2005) 249–259.
[17] M. Mezcua, I. Ferrer, M.D. Hernando, A.R. Fernández-Alba, Food Addit. Contam. 23 (2006) 1242–1251.
[18] R. Thiruvenkatachari, T.O. Kwon, I.S. Moon, Sep. Sci. Technol. 40 (2005) 2871–2888.
[19] J.-M. Lee, M.-S. Kim, B.-W. Kim, Water Res. 38 (2004) 3605–3613.
[20] K. Nomiyama, T. Tanizaki, T. Koga, K. Arizono, R. Shinohara, Arch. Environ. Contam. Toxicol. 52 (2007) 8–15.
[21] J.R. Peller, S.P. Mezyk, W.J. Cooper, Res. Chem. Intermed. 35 (2009) 21–34.

[22] C. Guo, M. Ge, L. Liu, G. Gao, Y. Feng, Y. Wang, Environ. Sci. Technol. 44 (2009) 419–425.
[23] R.A. Torres, J.I. Nieto, E. Combet, C. Petrier, C. Pulgarin, Appl. Catal., B: Environ. 80 (2008) 168–175.
[24] V. Maroga Mboula, V. Héquet, Y. Andrès, L.M. Pastrana-Martínez, J.M. Doña-Rodríguez, A.M.T. Silva, P. Falaras, Water Res. 47 (2013) 3997–4005.
[25] J.-C. Sin, S.-M. Lam, A.R. Mohamed, K.-T. Lee, Int. J. Photoenergy 2012 (2012).
[26] H. Tao, S. Hao, F. Chang, L. Wang, Y.R. Zhang, X.H. Cai, J.S.D. Zeng, Water Air Soil Pollut. 214 (2011) 491–498.
[27] D.P. Subagio, M. Srinivasan, M. Lim, T.-T. Lim, Appl. Catal., B: Environ. 95 (2010) 414–422.
[28] C. Jia, Y. Wang, C. Zhang, Q. Qin, S. Kong, S.K. Yao, Environ. Eng. Sci. 29 (2012) 630–637.
[29] Y. Ohko, I. Ando, C. Niwa, T. Tatsuma, T. Yamamura, T. Nakashima, Y. Kubota, A. Fujishima, Environ. Sci. Technol. 35 (2001) 2365–2368.
[30] N. Watanabe, S. Horikoshi, H. Kawabe, Y. Sugie, J.C. Zhao, H. Hidaka, Chemosphere 52 (2003) 851–859.
[31] S.Y. Wang, Photochemistry and Photobiology 1 (1962) 135–145.
[32] UV-Geräte zur Desinfektion in der Wasserversorgung, W 294-3, Bonn, 2006.
[33] D. Curco, J. Gimenez, A. Addardak, S. Cervera-March, S. Esplugas, Catal. Today 76 (2002) 177–188.
[34] U. Stafford, K.A. Gray, P.V. Kamat, J. Catal. 167 (1997) 25–32.
[35] W.-T. Tsai, C.-W. Lai, T.-Y. Su, J. Hazard. Mater. 134 (2006) 169–175.
[36] D. Zheng, N. Wang, X. Wang, Y. Tang, L. Zhu, Z. Huang, H. Tang, Y. Shi, Y. Wu, M. Zhang, B. Lu, J. Hazard. Mater. 199 (2012) 426–432.
[37] C.A. Staples, P.B. Dorn, G.M. Klecka, S.T. O'Block, L.R. Harris, Chemosphere 36 (1998) 2149–2173.
[38] J.W. Lee, T.O. Kwon, R. Thiruvenkatachari, I.S. Moon, J. Environ. Sci.—China 18 (2006) 193–200.
[39] A. Petrauskas, E. Kolovanov, Perspect. Drug Discovery Des. 19 (2000) 99–116.
[40] M.R. Hoffmann, S.T. Martin, W. Choi, D.W. Bahnemann, Chem. Rev. 95 (1995) 69–96.
[41] M. Sörensen, F.H. Frimmel, Water Res. 31 (1997) 2885–2891.
[42] J.S. Edmonds, M. Nomachi, M. Terasaki, M. Morita, B.W. Skelton, A.H. White, Biochem. Biophys. Res. Commun. 319 (2004) 556–561.
[43] A. Atkinson, D. Roy, Biochem. Biophys. Res. Commun. 210 (1995) 424–433.
[44] A. Atkinson, D. Roy, Environ. Mol. Mutagen. 26 (1995) 60–66.
[45] A. Izzotti, S. Kanitz, F. D'Agostini, A. Camoirano, S. De Flora, Mutat. Res. Genet. Toxicol. Environ. Mutagen. 679 (2009) 28–32.
[46] S. De Flora, R.T. Micale, S. La Maestra, A. Izzotti, F. D'Agostini, A. Camoirano, S.A. Davoli, M.G. Troglio, F. Rizzi, P. Davalli, S. Bettuzzi, Toxicol. Sci. 122 (2011) 45–51.
[47] X. Ye, X. Zhou, L. Needham, A. Calafat, Anal. Bioanal. Chem. 399 (2011) 1071–1079.
[48] Y. Li, B. Wen, C. Yu, C. Chen, H. Ji, W. Ma, J. Zhao, Chem. Eur. J. 18 (2012) 2030–2039.
[49] B. Ohtani, J. Photochem. Photobiol., C: Photochem. Rev. 11 (2010) 157–178.
[50] L.M. Dorfman, G.E. Adams, Reactivity of the hydroxyl radical in aqueous solutions, in: Report no. NSRDS-NBS-46, National Bureau of Standards, Washington, DC, 1973, pp. 22.
[51] D. Monllor-Satoca, R. Gomez, M. Gonzalez-Hidalgo, P. Salvador, Catal. Today 129 (2007) 247–255.